Lenis, JA.; Rico Tortosa, PM.; Gómez Ribelles, JL.; Pacha-Olivenza, MA.; González-Martín, ML.; Bolívar, FJ. (2020). Structure, morphology, adhesion and in vitro biological evaluation of antibacterial multi-layer HA-Ag/SiO2/TiN/Ti coatings obtained by RF magnetron sputtering for biomedical applications. Materials Science and Engineering C: Materials for Biological Applications (Online). 116:1-13. https://doi.org/10.1016/j.msec.2020.111268

Structure, morphology, adhesion and *in vitro* biological evaluation of antibacterial multi-layer HA-Ag/SiO_2/TiN/Ti coatings obtained by RF magnetron sputtering for biomedical applications

J.A. Lenis *[a], P. Rico[b,c], J.L. Gómez Ribelles [b,c], M.A. Pacha-Olivenza[c,d], M.L. Gonzáles-Martín [e,c], F.J. Bolívar [a].

[a] Centro de Investigación, innovación y Desarrollo de Materiales CIDEMAT, Facultad de Ingeniería, Universidad de Antioquia, Medellín, Colombia.

[b] Centre for Biomaterials and Tissue Engineering, CBIT, Universitat Politècnica de València, Spain.

[c] Biomedical Research Networking Center in Bioengineering, Biomaterials and Nanomedicine (CIBER-BBN), Valencia, Badajoz, Spain.

[d] Department of Biomedical Sciences, Faculty of Medicine and University Institute of Biosanitary Research of Extremadura (INUBE), University of Extremadura, Badajoz, Spain.

[e] Department of Applied Physics, Faculty of Science and University Institute of Biosanitary Research of Extremadura (INUBE), University of Extremadura, Badajoz, Spain.

***Corresponding author**

Email address: julian.lenis@udea.edu.co (J.A. Lenis).

Abstract

Biocompatible and antibacterial multi-layer coatings of hydroxyapatite (HA)-Ag/SiO_2/TiN/Ti were obtained on the Ti-6Al-4V alloy, by means of the magnetron sputtering technique. During characterization of the coatings, the chemical composition was

evaluated by energy dispersive X-ray spectroscopy and the phase analysis was carried out by X-ray diffraction. The morphology of the coatings was observed by field emission scanning electron microscopy, while transmission electron microscopy was used to appreciate their structure. The adhesion of the coatings to the substrate was evaluated by micro scratch test. The *in vitro* biological response was evaluated in terms of cytotoxicity, adhesion and differentiation of mouse mesenchymal stem cells, as well as adhesion and bacterial viability of *Staphylococcus aureus* strain. Through the compositional study carried out, the deposition of the HA phase was verified, with a Ca/P ratio close to 1.67 and the characteristic diffraction peaks of this compound. The structural study of the coatings evidenced the obtention of multi-layer architectures. The use of an intermediate SiO_2/TiN/Ti trilayer was found to improve adhesion between HA-Ag and the substrate by 84%. Finally, the *in vitro* biological tests carried out indicated a potentially non-toxic character in the coatings. Additionally, an antibacterial effect was registered at low concentrations of Ag (<0.25 mg/L).

Keywords: Magnetron sputtering; Multi-layer coating; Hydroxyapatite; Structure; Interface; *In vitro* biological properties.

1. Introduction

The combination of osseointegration and antibacterial properties in prosthetic implants such as microplates and fixation screws is widely desired, since adequate interaction between the incorporated material and the bone is essential for the mineralization process. In addition, the local action of antibacterial elements prevents the formation of bacterial infections that trigger major health problems and, in many cases, lead to removal of the implanted device

[1,2]. For these reasons, both properties are strongly linked to long-term success in surgical implantation procedures. For the elaboration of prosthetic implants, titanium alloys are commonly used. These have good mechanical properties, necessary in many areas of prosthetic replacement, and are also biocompatible, leading to good acceptance within the human body [3]. However, this material does not have antibacterial properties, so the implanted device is susceptible to bacterial colonization that can be induced even by the surgical procedure itself, by inadequate asepsis for example. Recent studies have focused on the surface modification of this alloy through the formation of a coating that enhances the biocompatibility of titanium and induces antibacterial properties in the implant. To achieve this, the magnetron sputtering (MS) technique is quite promising, since it allows the combination of elements by means of a simultaneous co-deposition or a multi-layer system, allowing coatings with good surface properties and high purity to be obtained [4–7]. Of the most widely used biocompatible materials in this type of coatings, calcium phosphates, especially hydroxyapatite (HA), have been of particular interest, since they have a great chemical similarity with bone mineral, favoring bone growth [8,9]. On the other hand, as a broad-spectrum antibacterial element, Ag is quite attractive [10–12]. However, this element can also cause cytotoxicity and, therefore, maximum concentration levels have been established, with some authors reporting values between 1-2.5 mg/L [13] and 10 mg/L [14,15]. The development of HA-Ag coatings by MS remains a work in progress, since it has not yet been possible to obtain complete control over characteristics such as the crystallinity and the Ca/P ratio of HA coatings, which influence the cell response of this material. M. Vallet-Regí *et al.* [16] found that, when the Ca/P ratio decreases below its stoichiometric value (1.67), the acidity and solubility increase, affecting its application in implants. In the literature there are reports for Ca/P ratios in HA coatings

with variations in a wide range from 1.3 to 3.8 [17,18]. Regarding crystallinity, some reports indicate that this property affects the dissolution of HA in the biological medium, meaning that amorphous coatings can affect the osteogenesis process [19]. Meanwhile, the adhesion strength between HA coatings and metal substrates is a great challenge, due to the dissimilar nature of both materials. For this reason, different intermediate layers between HA and Ti alloys have been studied. E. Mohseni *et al.* [20] increased adhesion between an HA coating obtained by MS and a Ti-6Al-4V substrate by 44.5% by incorporating a TiN intermediate layer. Like HA, this nitride is biocompatible and, additionally, has a high chemical stability, which makes it optimal for biomedical application [21]. D.A. Hamdi *et al*. [22] obtained an increase in the bond strength of an HA coating on a Ti-6Al-4V substrate by incorporating an intermediate Al_2O_3/TiO_2 bilayer deposited by MS. This behavior was associated with the structural similarity between the oxide layers and the substrate, as well as between their thermal expansion coefficients. The increase in adhesion of this type of system could also be associated to the diffusion of elements at the interface between the HA and the oxide layers during the deposition process or subsequent heat treatments [21,23]. However, there is a lack of studies that make it possible to appreciate in great detail the interface generated between HA and the intermediate layers and between these and the substrate. Additionally, there are very few studies related to the biocompatibility and antibacterial properties of multi-layer HA-Ag coatings, and none on the effect of the incorporation of intermediate layers on the biological response of this type of systems.

In the present study, an intermediate SiO_2/TiN/Ti trilayer was incorporated between a Ti-6Al-4V substrate and a multi-layer HA-Ag coating. The surface features, structure,

interface, adhesion to the substrate, Ag release, *in vitro* cell viability, adhesion and differentiation, and the antibacterial properties of the resulting system were analyzed, studying the effect of the incorporation of the trilayer.

2. Materials and methods

2.1. Deposition of the multi-layer coatings

HA-Ag/SiO_2/TiN/Ti multi-layer coatings were obtained on Ti-6Al-4V discs using a MS device couple to direct current (DC) sources (ADL, MARIS) and a radio frequency (RF) source (13.56 MHz, SEREM). High purity (> 99.9%) HA, Ag, Ti and Si targets, with dimensions of 500 × 100 × 6 mm^3, were used to obtain the multi-layer coatings. The substrates were subjected to *in situ* ionic cleaning before starting the deposition process, using high purity argon gas and a voltage of -750 V for 1 h. The deposition temperature and the working pressure were fixed at 250 °C and 0.5 Pa, respectively. Table 1 shows the remaining process parameters, which were chosen based on previous works [24,25]. Figure 1 shows the architecture of the system developed, consisting of a SiO_2/TiN/Ti trilayer joined both to a multi-layer HA-Ag coating and a Ti-6Al-4V substrate. Considering that HA can be dissolved in a biological medium, the multi-layer coating consists of alternating HA and Ag layers to guarantee a long-term antibacterial effect. Additionally, an HA-Ag system was obtained directly on the substrate for comparative purposes.

Table 1. Process parameters used to obtain the multi-layer coatings.

Coatings	Power DC (W)	Power RF (W)	Target-substrate distance (cm)	Atmosphere	Bias (V)	Total layers	Total time (min)
Ti	1200	---	8	Ar	-70	1	10
TiN				$Ar + N_2$ (2:1)			60
SiO_2	600			$Ar + O_2$ (3:1)			90
HA	---	600	4	Ar	-20	5	300
Ag	20	---				4	12

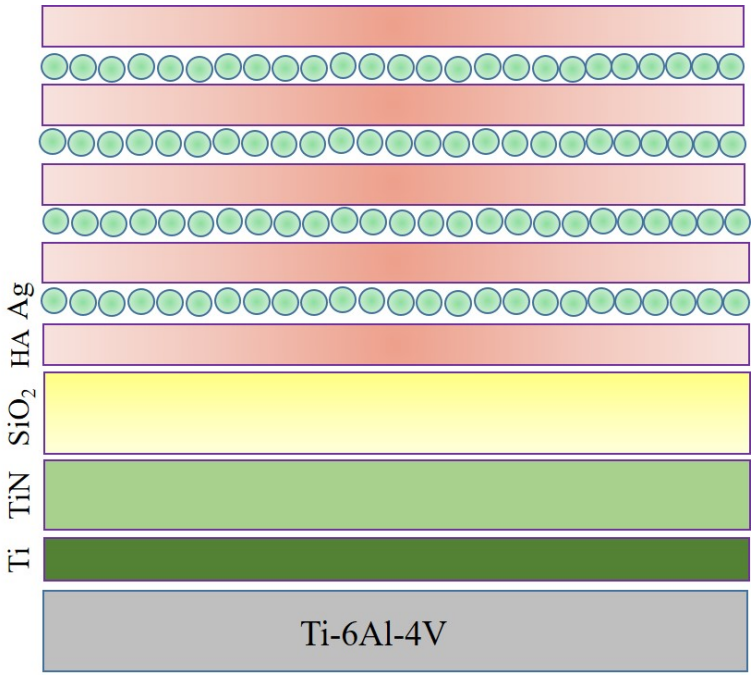

Figure 1. Architecture designed of the system developed.

2.2. Coatings characterization

2.2.1. Elemental composition, crystallinity, morphology and structure

The elemental composition of the multi-layer systems was measured by energy dispersive X-ray spectroscopy (EDS, Oxford instruments X-Max 80), with resolution of 126 eV. Phases were evaluated by X-ray diffraction (XRD) using a Panlitycal X´pert pro MPD equipment in reflection mode, with Cukα radiation λ=1.540598 Å at 45 kV and 40 mA, analyzing from 20° to 68° (2Θ) at a scanning speed of 1°/min. Additionally, the crystallite size was calculated according to the Scherrer equation [26]. The morphology of the coatings was appreciated by field emission electron microscopy (FESEM) (ZEISS Gemini-SEM500, 2 kV). Additionally, grain sizes were calculated from FESEM images using linear intercept method [27]. The structure of the coatings was observed by transmission electron microscopy (TEM) and scanning transmission electron microscopy (STEM) (JEOL-JEM-2100F, 200 kV). For this, a cross-sectional lamella with dimensions of 5 × 5 μm^2 and thickness less than 100 nm was obtained by focused ion beam (ZEISS AURIGA, 30 kV, 500 pA).

2.2.2. Surface features

The roughness of the coatings and the substrate was measured in triplicate by atomic force microscopy (AFM) (MFP-3D Infinity). The evaluated area was fixed at 5 × 5 μm^2. Meanwhile, the wettability and surface free energy were determined according to the procedure previously described in [28].

2.2.3. Adhesion

The critical load (L_C) related with the adhesive failure of the coatings was measured in triplicate by micro-scratch tests using a nanoindentation device (MTS´s XP System Corporation) equipped with a conical diamond tip with 10 μm in diameter. A progressive load up to 500 mN was applied, with an increase rate of 3.21 mN/s. The evaluated distance was fixed at 2000 μm.

2.2.4. Ag release

To determine the Ag release from the coatings, three samples of each system were immersed in phosphate buffered saline (PBS) medium at 37 °C as described in [29] but here we evaluated also 72 and 720 h of exposure. The measures were performed by atomic absorption spectrophotometer with an Ag lamp using a Thermo Electron Corporation S4 equipment.

2.2.5. *In vitro* biological evaluation

The coatings and the Ti-6Al-4V substrate were ultraviolet sterilized in a horizontal laminar flow cabinet for 50 min prior to cell and bacterial seeding. For cell viability, adhesion and differentiation assays, mouse mesenchymal stem cells (mMSCs) (C3H10T1/2 cells from RIKEN Cell Bank, Japan) were used. The strain used for bacterial adhesion and viability tests was *Staphylococcus aureus* ATCC 29213 (*S. aureus*) from the Spanish Type Culture Collection (CECT). All assays were performed in triplicate.

2.2.5.1. Ag cytotoxicity test

Ag cytotoxicity was evaluated by MTT (3-(4,5-dimethylthiazol-2-yl)-2,5-diphenyl tetrazolium bromide) assay (Roche). mMSCs with a density of 10.000/cm^2 were seeded in culture plates with cell culture medium consisting of Dulbecco's Modified Eagle Medium (Invitrogen) supplemented with 10% fetal bovine serum and 1% penicillin/streptomycin at 37 °C and 5% CO_2 for 24 h. After, this medium was replaced by culture medium containing AgCl, which was added to obtain Ag^+ concentrations from 0.06 to 14.64 mg/L, which were defined according to results registered for the Ag release assay and some reports in the literature [14,30]. Thereupon, an incubation for 72 h was carried out. Subsequent, MTT was added to the samples and a new incubation for 4 h was performed. 20% dimethyl sulfoxide was used to treat the cytotoxic control. To measure the absorbance at 570 nm, a spectrophotometer (Perkin Elmer Precisely, VICTOR^3) was used.

2.2.5.2. Coatings cytotoxicity

The coatings cytotoxicity was evaluated in non-contact mode by MTT assay. For this, both the coatings and substrate (control) were incubated in cell culture medium at 37 °C for 72 h. After, this medium was taken to culture plates with previously seeded cells at density of 10.000/cm^2, thereupon a new incubation was carried out for further 72 h. Then, the protocol described above in section 2.2.5.1 was followed.

2.2.5.3. Cell adhesion

mMSCs were seeded at a density of 5.000/cm^2 on the surface of the coatings and the substrate in cell culture medium at 37 °C and 5% CO_2 for 3 and 24 h. After each culture, samples were washed, fixed and permeabilized as described in [30]. For the immunostaining procedure, samples were incubated in primary antibody anti-vinculin (Sigma) dil. 1:400 in blocking solution consisting of Dulbecco's phosphate buffered saline (Invitrogen) supplemented with 2% Bovine Serum Albumin (Sigma) for 1 h. After a new wash, samples were incubated in secondary antibody Alexa Fluor 555 anti-mouse and Alexa Fluor 488 Phalloidin, dil. 1:700 and 1:100, respectively in blocking solution for 1 h. Samples were washed again prior to assembly with Vectashield-DAPI (Vector laboratories). Finally, all samples were observed under Nikon Eclipse 80i fluorescence microscope.

2.2.5.4. Cell differentiation

mMSCs were seeded at a density of 20.000/cm^2 on the surface of the coatings and the substrate in culture medium at 37 °C and 5% CO_2 until reach confluence. After 48 h, cells were stimulated with osteogenic differentiation medium for 15 days as described in [30]. An immunostaining similar to that explained above in section 2.2.5.3 was performed, but this time using the antibodies described in Table 2. Osteopontin (OPN) and Integrin binding sialoprotein (IBSP) were used as osteogenic markers.

Table 2. Antibodies used for cell differentiation assay.

Osteogenic differentiation	Primary antibody	Secondary antibody
OPN	OPN anti mouse, Santa Cruz, Biotechnology, dil. 1:200.	Alexa Fluor 555 α-mouse, 1:700 and Alexa Fluor 488 Phalloidin, dil. 1:100.
IBSP	IBSP anti rabbit, dil. 1:200.	Alexa Fluor 555 goat anti-rabbit,1:700 (Live Technologies) and Alexa Fluor 488 Phalloidin, dil. 1:100.

2.2.5.5. Antibacterial properties

S. aureus strain suspensions at concentration of 3×10^8 bacteria/mL were kept in contact with the surface of the coatings and the substrate for 1, 2 and 4 h. The assay was carried out as described in [31].

2.2.6. Image analysis

Image acquisition for viability, adhesion and cell differentiation assays was performed at 10x and 40x with n = 20. Images were processed using the Fiji-Image J software. Bacteria quantification was performed with 10 images per sample at 100x using the NIS Elements Br software (Nikon Instrument Inc., NY, USA).

2.2.7. Statistical analysis

The results obtained are shown as the mean ± standard deviation. The results of cell viability were analyzed by one-way analysis of variance using the GraphPad Prims 6 XML software.

3. Results and discussion

3.1. Elemental composition, crystallinity, morphology and structure

Table 3 shows the Ca/P ratio and the Ag atomic percentage for multi-layer coatings of HA-Ag/SiO_2/TiN/Ti and HA-Ag. The Ca/P ratio is slightly higher in the HA-Ag system obtained on the intermediate bilayer than in the system deposited directly on the substrate, with respective values of 1.73 and 1.67. Alterations in the elemental composition of HA films obtained by MS have been widely reported in the literature, with variations from 1.4 to 3.8 in the Ca/P ratio [17,18], where it has been shown that the substrate surface charge, modified by a bias voltage, can generate phosphorus resputtering, leading a reduction of the Ca/P ratio in HA coatings. This could indicate that SiO_2/TiN/Ti trilayer acted as an electrical barrier, which decreased the effect of the substrate surface charge on the phosphorus resputtering. On the other hand, the N/Ti and O_2/Si ratios obtained indicate excellent compositional control, since the values obtained were close to the stoichiometric values for both compounds.

Table 3. Chemical composition analysis of the deposited coatings: HA-Ag and HA-Ag/SiO_2/TiN/Ti.

Coatings	N/Ti ratio	O_2/Si ratio	Ca/P ratio	Ag atomic %
HA-Ag/SiO_2/TiN/Ti	1.15	1.89	1.73	4.7 ± 0.01
HA-Ag	---	---	1.67	4.5 ± 0.01

Figure 2 shows the XRD study of the multi-layer coatings. There, peaks related to planes (200) and (220) of Ag and peaks of Ti associated with the substrate are observed. Regarding HA, a preferential growth along plane (112) is observed, which was not altered by the change to the surface where it was deposited. However, the type of surface did have an effect on the crystallinity of this compound. This was evidenced by the greater intensity in the peaks related to planes (112) and (002) of HA for the coating deposited on the SiO_2/TiN/Ti trilayer, where a third peak associated with plane (211) of this same compound is also observed. It is important to note that the peaks associated with HA are slightly wide, which could indicate that nanocrystalline coatings were obtained [32]. This was verified by calculating the crystallite size for each system, where values of 29.3 and 31.9 nm were obtained respectively for the HA-Ag and HA-Ag/SiO_2/Ti/Ti coatings. These values are higher than those obtained in some similar studies with HA [33,34]. Regarding the behavior obtained, it has been found in the literature that the decrease or increase in the crystallite size could be related to the polarization of the substrate. A.A. Ivanova *et al.* [32] obtained a transition from a nanocrystalline to amorphous structure in an HA coating, after polarizing the substrate with a voltage of -50 V. The crystallite size reported was 26 nm. This could

indicate that the behavior shown in the present work is also associated to modifications in the Ti-6Al-4V surface charge through the deposition of the SiO_2/TiN/Ti trilayer.

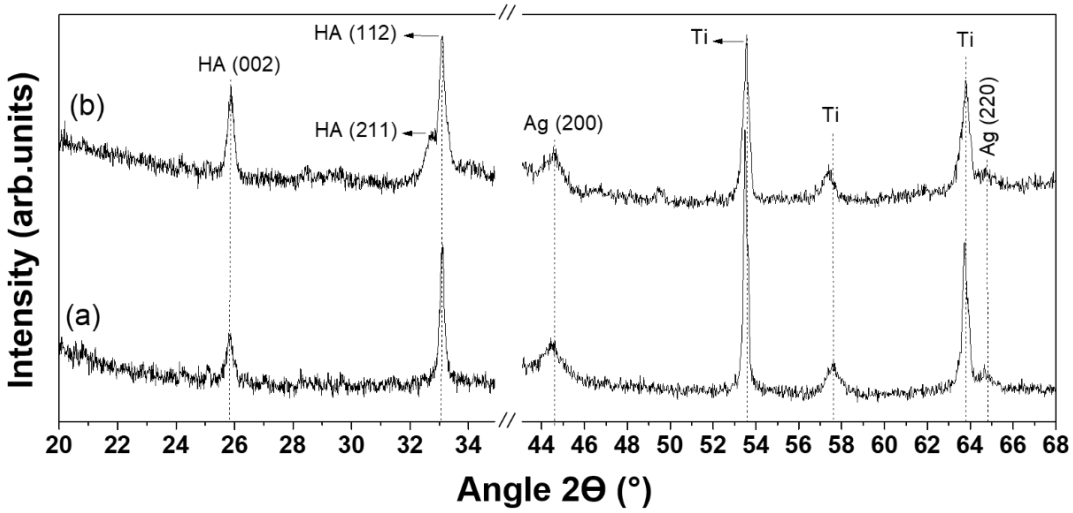

Figure 2. Diffractogram of the deposited coatings: a) HA-Ag and b) HA-Ag/SiO_2/TiN/Ti.

Figure 3 shows the surface morphology and cross-sectional view of the multi-layer coatings of HA-Ag (Figure 3a) and HA-Ag/SiO_2/TiN/Ti (Figure 3b). For both systems, grain morphology is observed at surface level, with an average size slightly smaller for the HA-Ag coating obtained on SiO_2/TiN/Ti (113 ± 23 nm) than in the HA-Ag system deposited directly on the Ti-6Al-4V (134 ± 30 nm). Meanwhile, the cross-sectional images obtained by TEM reveal the structure of both multi-layer systems. For the HA-Ag coating (Figure 3a), 5 dense and uniform layers of HA of approximately 90 nm thickness each, and 4 intermediate layers of Ag of approximately 30 nm thickness each are seen. The high irregularity in the Ag layers indicate that there was an Ag diffusion towards the adjacent HA layers during the deposition process. Figure 3b shows that the HA-Ag coating and the

SiO_2/TiN/Ti trilayer are perfectly bonded to both the substrate and the first layer of HA. The SiO_2 layer has a thickness close to 160 nm and a dense and amorphous structure, while the TiN layer has a thickness of approximately 100 nm and a columnar growth is appreciated, which is characteristic of this compound when it is deposited by MS [20,35]. Additionally, there is a lack of reports about the growth of HA-Ag systems on nitrides or oxides surfaces, since this coating is usually deposited directly on metal substrates [36,37]. Finally, the initial Ti layer has a thickness close to 80 nm. To enhance the adhesion between a specific coating and substrate, the intermediate layers used must be of low thickness since, when this is increased, both the residual stresses and the number of defects at micro or nanometric scale can also increase. For this reason, anchor layers with a thickness less than 200 nm are normally used, according to the literature [20,38].

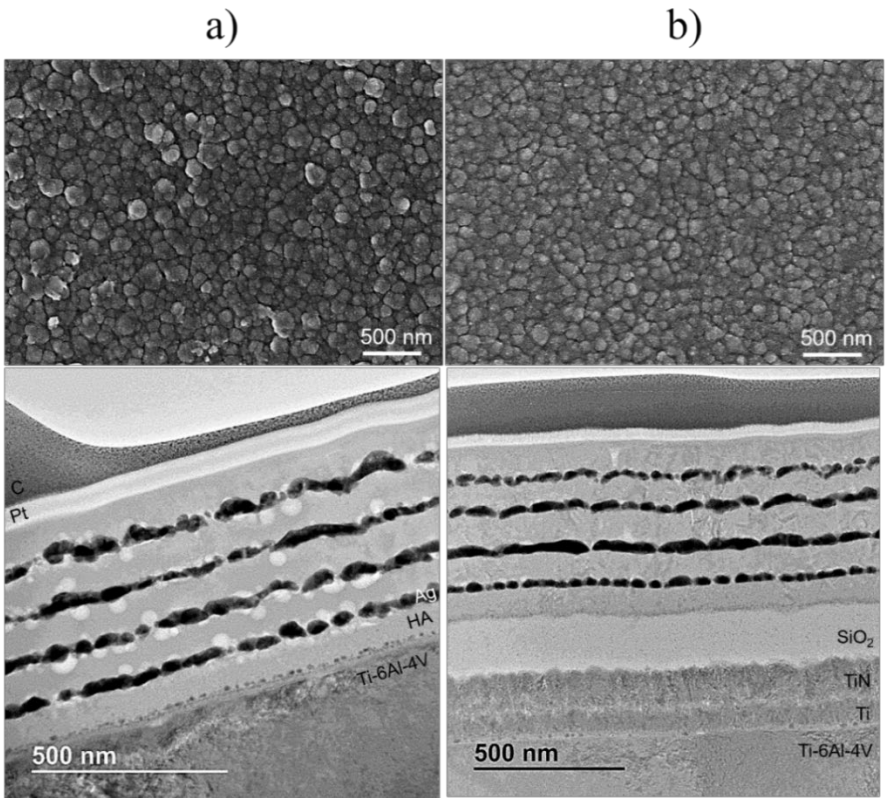

Figure 3. Surface morphology (FESEM) and cross-section view (TEM) of the deposited coatings: a) HA-Ag and b) HA-Ag/SiO_2/TiN/Ti.

Figure 4 shows the structure as observed by STEM of the coatings of HA-Ag (Figure 4a) and HA-Ag/SiO_2/TiN/Ti (Figure 4b). There, the chemical composition evaluation zones for both systems performed by EDS are observed, the results of which are summarized in Table 4. For the HA-Ag system, it is observed that, at the interface between Ti-6Al-4V and the first HA layer (Spectrum 1), there is a presence of both elements of the HA coating (Ca, P and O), as well as of the substrate (Ti and Al). This indicates that there was diffusion of these last two elements towards the first HA layer, generating the transition interface observed in the left image of Figure 4a. In the multi-layer HA-Ag/SiO_2/TiN/Ti coating, an alteration at the interface between HA and the substrate is again appreciated, as shown in

the left image of Figure 4b, where some grains can be seen. This, according to Spectrum 2, could indicate the formation of a titanium oxide as an effect of the temperature applied during the deposition process [34]. In the right image of Figure 4b, two transition zones of approximately 20 nm thickness each are observed, which correspond to the interface between TiN and el SiO_2, and between SiO_2 and the initial HA layer. Spectrum 3, associated with the first zone, indicates the presence of both elements Ti and N, as well as Si and O, both compounds with a slightly altered stoichiometry. Spectrum 4 indicates the presence of the elements Ca, P, O and Si, indicating the possible diffusion of Si and O towards the HA layer by chemical affinity.

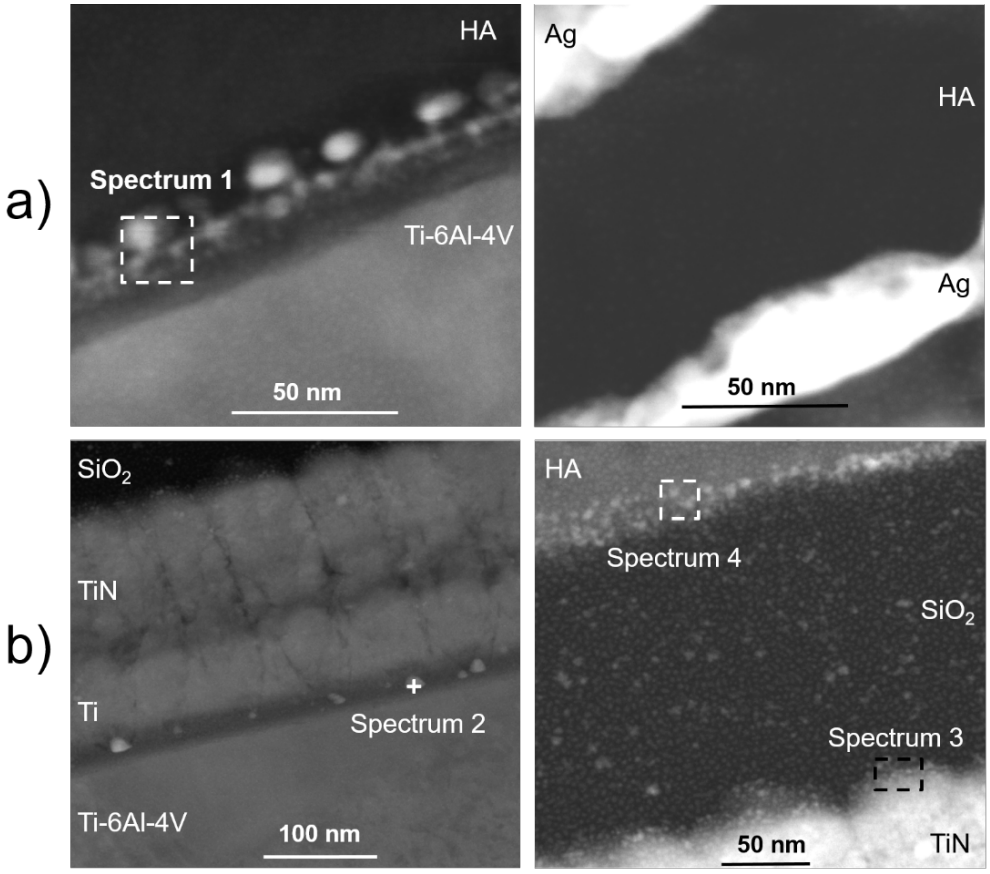

Figure 4. Cross-section view of the deposited coatings obtained by STEM: a) HA-Ag and b) HA-Ag/SiO_2/TiN/Ti.

Table 4. Chemical composition analysis performed by EDS at the interface between the deposited layers.

Spectrum N°	Atomic %							
	Ca	P	O	Ti	Al	V	N	Si
1	26.5	7.0	49.8	10.2	6.5	---	---	---
2	---	---	12.3	79.8	4.8	3.1	---	---
3	---	---	32.2	24.1	---	---	26.2	17.5
4	15.9	6.4	63.2	---	---	---	---	14.5

3.2. Roughness, wettability and surface free energy

Figure 5 shows the results of the roughness study carried out by AFM on the developed coatings. Initially, 3D images are observed for the surface of each of the systems. These show grain morphologies for the developed coatings which had been previously appreciated by FESEM study. However, it is appreciated that the HA-Ag system obtained on the trilayer is in the form of islands located in different regions of the evaluation area. Meanwhile, the root mean square (RMS) roughness values are presented in the graph, where the horizontal broken lines indicate the RMS values of the intermediate layers used and the substrate. The substrate had the lowest value (3.9 nm), followed by the TiN layer with 8.6 nm and the SiO_2/TiN/Ti trilayer with 20.7 nm. The roughness of the HA-Ag system was affected by the surface where it was deposited, the lowest value being obtained for the HA-Ag coating obtained on the substrate, with 10.8 ± 1.6 nm, while this same system deposited on the trilayer presented a value of 27.4 ± 2.1 nm. The increase in roughness could be favorable for the biological response of this type of surface, in terms of

adhesion, proliferation and cell differentiation [9,39]. Since rough surfaces favor the absorption of proteins such as fibrin and the adhesion of osteogenic cells [40]. Similar RMS values to those obtained in the present study were obtained by other authors [41,42].

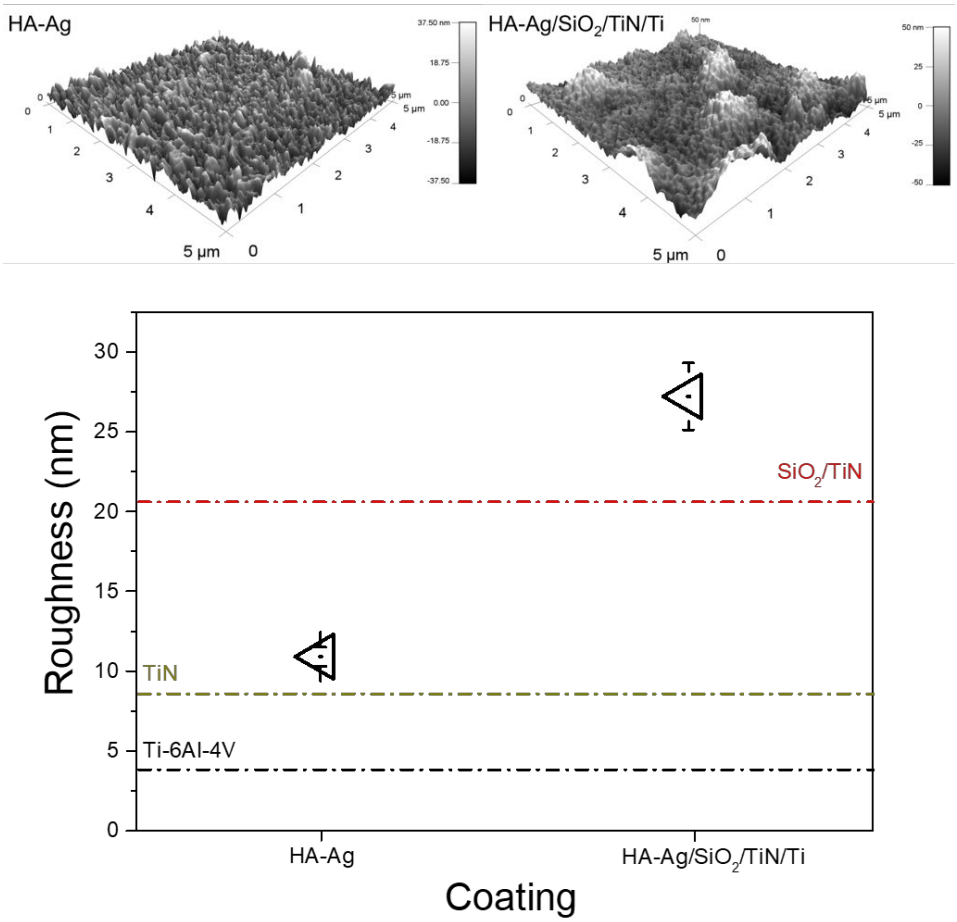

Figure 5. Roughness of the deposited coatings: HA-Ag and HA-Ag/SiO_2/TiN/Ti. The roughness values for Ti-6Al-4V substrate and for TiN and SiO_2/TiN/Ti coatings are marked by dashed lines.

The water contact angle values and the surface free energy calculated for the developed coatings and the substrate are shown in Figure 6. There, it is appreciated that both the substrate and the coatings obtained have a hydrophilic character [30], since the water contact angle is less than 90°. However, the graph shows that the substrate is very close to this value, while the coatings have a higher affinity for water, with values between 63° and 69°. The behavior obtained could be associated to the presence of phosphate and hydroxyl anions in the HA coatings, which tend to strongly attract H^+ of H_2O molecules [43]. Hydrophilic surfaces tend to exhibit good cell adhesion and differentiation [44,45]. On the other hand, the lowest surface free energy was obtained for the substrate, which was increased close to 34% through the deposition of the multi-layer coatings.

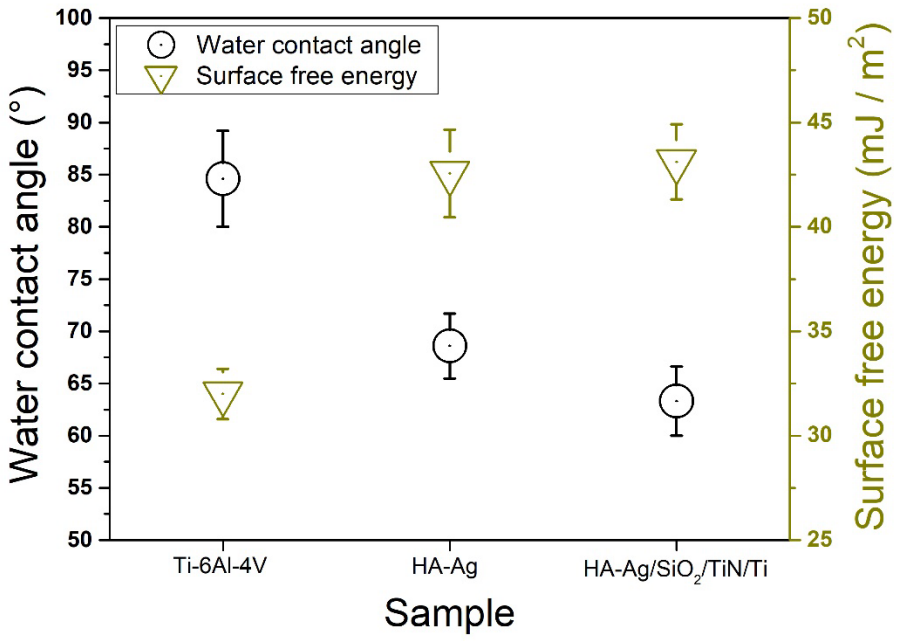

Figure 6. Water contact angle and surface free energy of the Ti-6Al-4V substrate and the deposited coatings: HA-Ag and HA-Ag/SiO_2/TiN/Ti.

3.3. Adhesion

The results of the micro-scratch test carried out on the surface of the developed systems are shown in Figure 7. There the friction registers and the normal load applied in function of the lateral distance that allowed the L_C values to be determined are observed. This, according to ASTM C1624-5 [46], is related to the adhesive failure of the coatings. The mechanical stress induced from the surface by the diamond tip is transmitted to the interface between the coating and the substrate and, if the bonding force is less than the magnitude of the shear stress, adhesive failure of the coating is generated. For the HA-Ag system, an abrupt change in the friction coefficient was registered at a distance of 650 μm. This indicates that at this point there was a change of the surface in contact with the tip, which is related to a coating-substrate transition at a L_C value of 114 mN, as can be observed in the corresponding image. From this point, some fluctuation in a wide range are observed, which is due to the influence of the substrate and removed material from the coating. An increase by 84% in the L_C was obtained by incorporating the SiO_2/TiN/Ti intermediate trilayer, reaching a L_C value of 210 mN. The failure of this system was at a distance of 1190 nm, as indicated by friction registers and the corresponding scratch image. The behavior obtained could be associated with the diffusion of elements at the interface between the HA and the SiO_2 layer during the deposition process, as appreciated in Figure 4, which favors bond strength [22]. We also believe that the result is related to a decrease in the residual stresses through energy dissipation in the trilayer used, as was obtained in [28] by incorporating a TiN/Ti bilayer. This decreases the magnitude of the stress between the first layer of the coating and the substrate. Another important aspect is the increase in the number of interfaces, which may deflect micro-cracks, favoring the adhesion strength. W. Boonrawd *et al.* [47] and A. Quirama *et al.* [42] reported L_C values lees than 130 mN in

HA coatings obtained on Ti substrates, which are lower than those registered for the HA-Ag/SiO_2/TiN/Ti system.

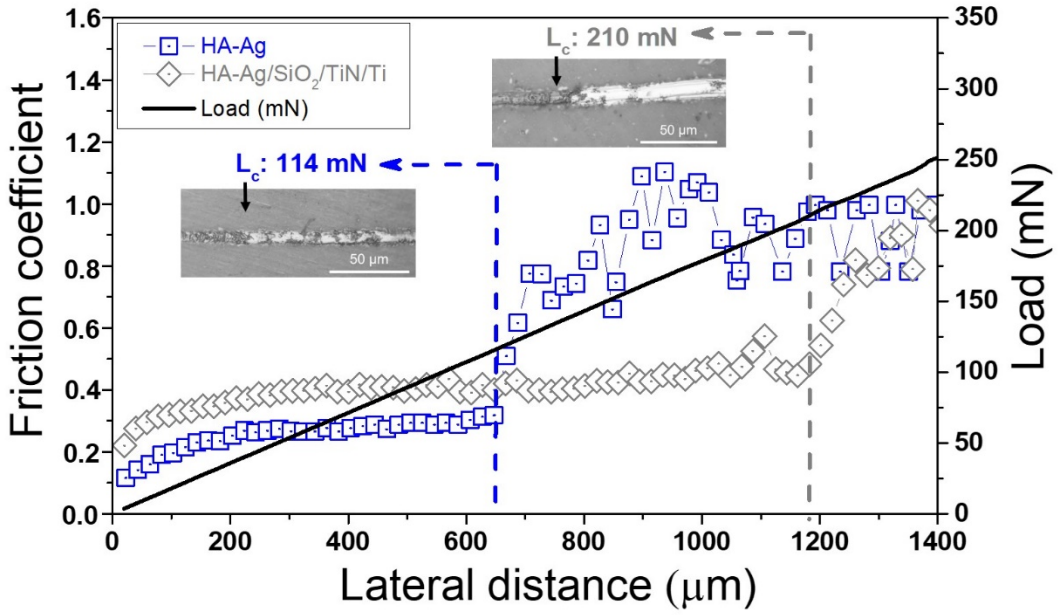

Figure 7. Scratch test of the deposited coatings: HA-Ag and HA-Ag/SiO_2/TiN/Ti.

3.4. Ag release in PBS

Figure 8 shows the results obtained for the Ag release test of the developed coatings. Figure 8a shows the Ag cumulative concentration. An increase is observed in this variable as a function of time for the two systems studied, indicating continuous Ag release from the coatings into the PBS medium. The Ag cumulative concentration from the HA-Ag system deposited on the trilayer was lower than that of the coating deposited directly on the substrate, reaching a reduction close to 50% in the last measurement at 720 h of evaluation.

The Ag release could be related to the crystallinity of the coatings, since its release to the medium is influenced by the dissolution or infiltration of HA. For this reason, the lowest Ag concentrations, related to a lower release of this element into the medium, were registered for the HA-Ag system deposited on the SiO_2/TiN/Ti trilayer, which presented the highest crystallinity degree. The values recorded during this test, with a maximum close to 0.21 mg Ag/L, are lower than those obtained by other authors for Ag release from coatings [48]. Figure 8b shows the Ag release in PBS medium. A decreasing trend in the Ag release rate to the medium is observed in the coatings developed, with the maximum value recorded during the initial measurement at 72 h of immersion, where the HA-Ag system presented a higher value than the HA-Ag/SiO_2/TiN/Ti coating. The graph shows that, at 192 h of evaluation, there is a significant reduction in the Ag release rate in both systems. From this point some fluctuations in a low range are observed and, finally, similar release values are observed for the coatings. The results obtained indicate the obtention of a prolonged Ag release, which could favor the antibacterial action over time. This is widely desired, since infections can appear many years after an implantation procedure [49,50].

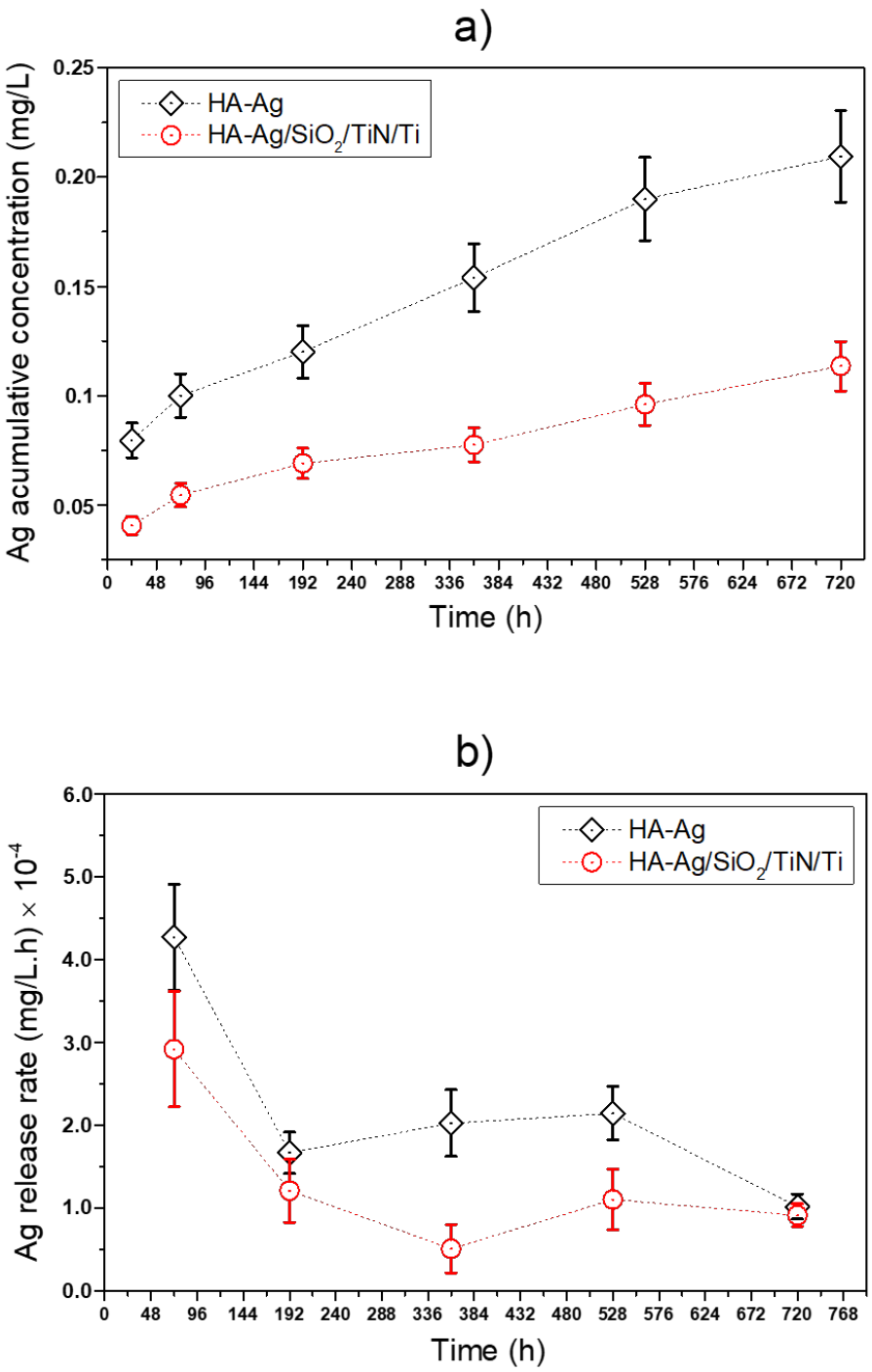

Figure 8. Ag release in PBS of the deposited coatings: HA-Ag and HA-Ag/SiO_2/TiN/Ti, a) accumulative concentration and b) release rate, of the deposited coatings: HA-Ag and HA-Ag/SiO_2/TiN/Ti.

3.5. Ag cytotoxicity assay

The results of the Ag^+ cytotoxicity assay on mMSCs used for the biological evaluation of the developed coatings are shown in Figure 9. There, the cell viability as a function of the increase in the Ag^+ concentration in the medium is observed, compared with a control of Ag free medium. It can be seen that the cells exposed to the medium with Ag^+ at low concentrations (up to 0.96 mg/L), present a morphology similar to that obtained in the control, and cell viability of 84%. However, from this point some dead cells are observed, the number of which increases proportionally to the Ag^+ concentration in the medium: for 1.83 mg/L a viability less than 40% is registered, reaching 1% for the maximum concentration (14.64 mg/L). These results show the cytotoxic effect of highly reactive Ag^+, which at certain concentrations can easily penetrate the membrane of cells, causing their death.

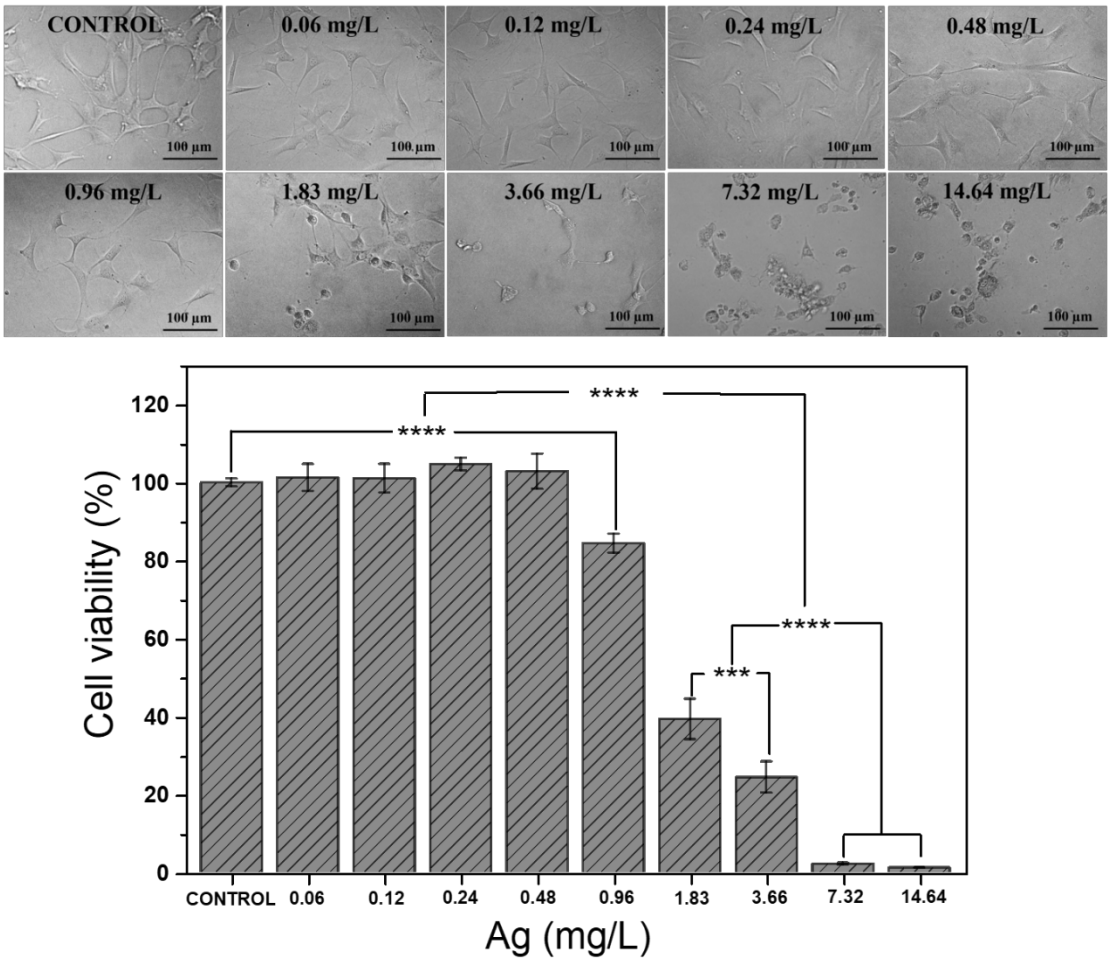

Figure 9. Cell viability test of the Ag^{+} in different concentrations. Data is represented as mean ± standard deviation. Significant values as ****P< 0.0001, ***P< 0.001.

3.6. Cell viability, adhesion and differentiation

The cell viability of the developed coatings and the Ti-6Al-4V substrate, which was used as a control, are shown in Figure 10. There, viability of 82% is observed for the HA-Ag coating, while viability of 105% is observed for the HA-Ag/SiO_2/TiN/Ti system. This behavior is due to the fact that the Ag^{+} release of the latter system was lower than that of the HA-Ag coating deposited directly on the substrate, which is related to the crystallinity

of the coatings, which was greater in the HA-Ag system obtained on the trilayer. This impeded Ag^{+} release into the medium during the assay, favoring the integrity of the mMSCs.

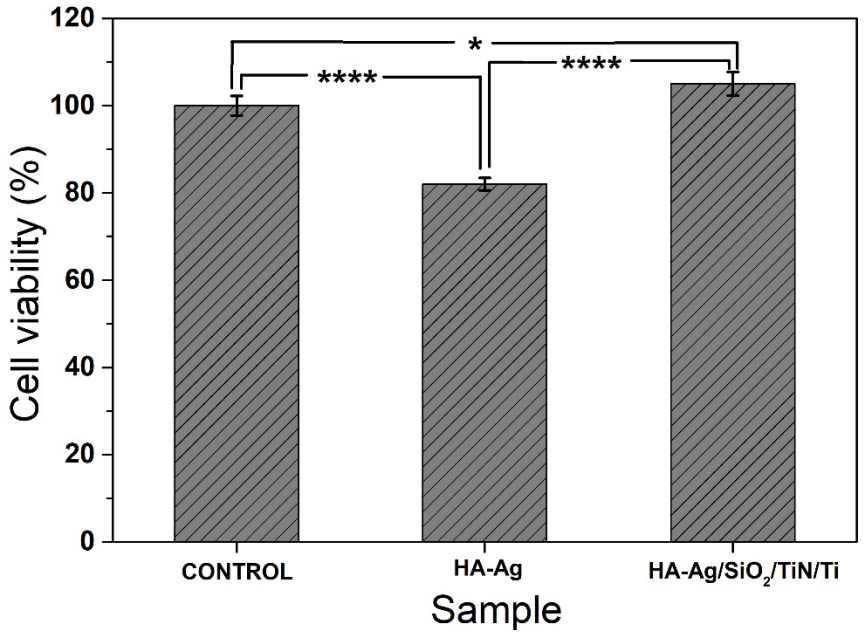

Figure 10. Cell viability test of the deposited coatings. Data is represented as mean ± standard deviation. Significant values as ****P < 0.0001, *P < 0.1.

Figure 11 shows the results of the adhesion test of mMSCs on the Ti-6Al-4V (control), and the developed coatings at times of 3 and 24 h. Figure 11a shows the images of the cells, where details such as the nucleus, morphology and focal adhesions are observed. This was achieved by detecting the following proteins: I) actin, the protein of which the cell´s cytoskeleton is composed, allowing the observation in great detail of its morphology; and II) vinculin, the protein secreted during the cell's adhesion process on a surface. The results

obtained indicate that there was an appropriate development of the cytoskeleton of the cultured cells both on the control surface and on the developed coatings. Furthermore, it can be seen that, with the increase in culture time, the cells present a more extended morphology and an increase in focal adhesions. Figure 11b shows the cell expansion area as a function of the type of surface used and the exposure time. There, it is observed that the mean area of expansion of mMSCs on the substrate and the HA-Ag/SiO_2/TiN/Ti coating was greater than in the HA-Ag system, which could be associated to greater Ag^+ release in this last coating. Based on these results, it is observed that Ag^+ slightly affects the growth of mMSCs, decreasing by approximately 20% its expansion area compared to the control and the system obtained on the SiO_2/TiN/Ti trilayer, which is associated with direct contact between the cells and the released Ag^+. Meanwhile, an increase in the expansion area with the exposure time was obtained during the adhesion test. Figure 11c shows the cell´s circularity as a function of the type of surface and the exposure time. It is observed that, at 3 h, the circularity values are similar in all evaluated samples. Additionally, the graph shows a large decrease (greater than 50%), in the circularity between 3 and 24 h of adhesion for all samples, indicating that the adhesion process was improved with the increase in the assay time, obtaining more extended cells and slightly circular morphologies. For 24 h, the results showed differences between the control and the HA-Ag coating, which presented the highest value. In Figure 11d the focal adhesion area for the evaluated samples as a function of the time is observed. At 3 h, similar values were observed for the coatings compared to the Ti-6Al-4V control. However, a large increase was recorded with increasing time up to 24 h for all systems. Finally, similar behavior was observed for the focal adhesion number, Figure 11e. The formation and establishment of these focal adhesions is a very important process in the adhesion of mMSCs on the

developed coatings, in which a process of integrin grouping begins and stable bonds are later generated between the proteins of the extracellular matrix and the cell cytoskeleton [51]. The analysis of the parameters presented above for mMSCs indicates that the adhesion of these cells to the surface of the evaluated samples is mainly influenced by the presence of Ag^{+}, released by the infiltration of HA layers, which affected to some extent the adequate development of the cytoskeleton and the cell adhesion to the HA-Ag system. On the other hand, surface characteristics such as roughness could also have contributed to the cell adhesion response. This, together with the lower Ag^{+} release obtained for this system, could explain the performance obtained by the HA-Ag coating deposited on the SiO_2/TiN/Ti trilayer, which presented the highest RMS value. Cells tend to spread principally on rough and hydrophilic surfaces [52,53]. In the present work, no clear trend was observed regarding surface features such as wettability and surface free energy of the developed systems and the adhesion of mMSCs. However, the recorded values (from 63° to 69°), are similar to those obtained by other authors, with good results in terms of cell adhesion and proliferation [54,55].

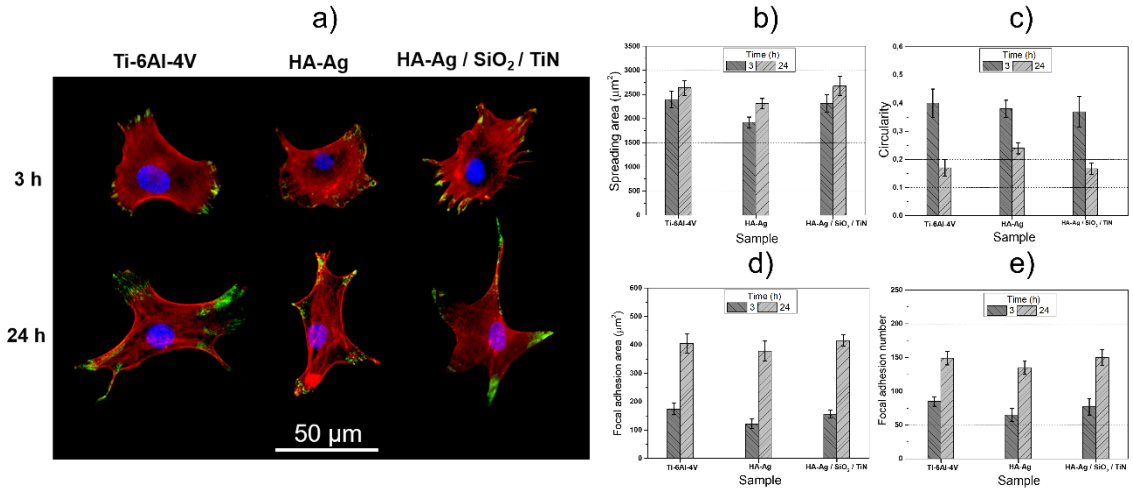

Figure 11. Adhesion of mMSCs on the different coatings and Ti-6Al-4V substrate: a) actin cytoskeleton (red), vinculin highlighting focal adhesions (green), nucleus stained with DAPI (blue), b) spreading area, c) circularity, d) focal adhesion area and e) focal adhesion number. Data is represented as mean ± standard deviation.

The results of the differentiation test of mMSCs on the substrate and the developed coatings are shown in Figure 12. The cell nucleus (blue) and the staining generated for both osteogenic markers used (green) are shown in Figure 12a. OPN promotes the osteoblastic phenotype, and its expression produces a secreted adhesive protein that is essential for adhesion, migration and cell survival. IBSP is present in the bone matrix and is characterized by binding to the HA of the bone, favoring early cell mineralization. Both proteins were detected in the samples, and their expression was quantified and is presented in Figure 12b. For OPN, similar expression levels are observed for the control and the HA-Ag system deposited on the trilayer, while the lowest levels were registered for the HA-Ag coating obtained directly on the substrate. Similarly, for the IBSP the lowest expression is observed for this system. The behavior obtained again indicates a relationship between the

cell response and the presence of Ag^+ on the surface of the coatings. Meanwhile Figure 12c presents the nucleus number for each system during 15 days of evaluation. There, a reduction close to 20% is observed for both the OPN and IBSP assays, which could indicate that, in the long term, cell proliferation is affected by the prolonged Ag^+ release. The results obtained in the present study against the two evaluated markers indicate that the coatings induce differentiation of mMSCs towards bone cells, showing good levels of staining for both OPN and IBSP. Furthermore, as in the cytotoxicity and cell adhesion assays, it is observed that Ag^+ does not greatly affect the cell response of the coatings, given that the Ag amount present at the surface level and its release rate are not very high. There is a lack for studies about the cell differentiation in HA-Ag multi-layer systems. However, the effect of Ag^+ on the differentiation of some cell types has been studied in recent years. C. Sengstock *et al*. [56] evaluated the effect of Ag nanoparticles (80 nm in diameter) on the viability and differentiation of human mesenchymal cells, finding cytotoxic effects for Ag nanoparticle concentrations $\geq$ 20 mg/L, and for Ag^+ concentrations $\geq$ 1.5 mg/L. In another study, A.M. Echavarría *et al.* [30] reported a decrease in the OPN expression in TaN coatings doped with Ag nanoparticles. This effect was found as the amount of Ag increased at the surface level. Ag nanoparticles have multiple effects on cell physiology and signal transduction, which can induce alterations in gene expression.

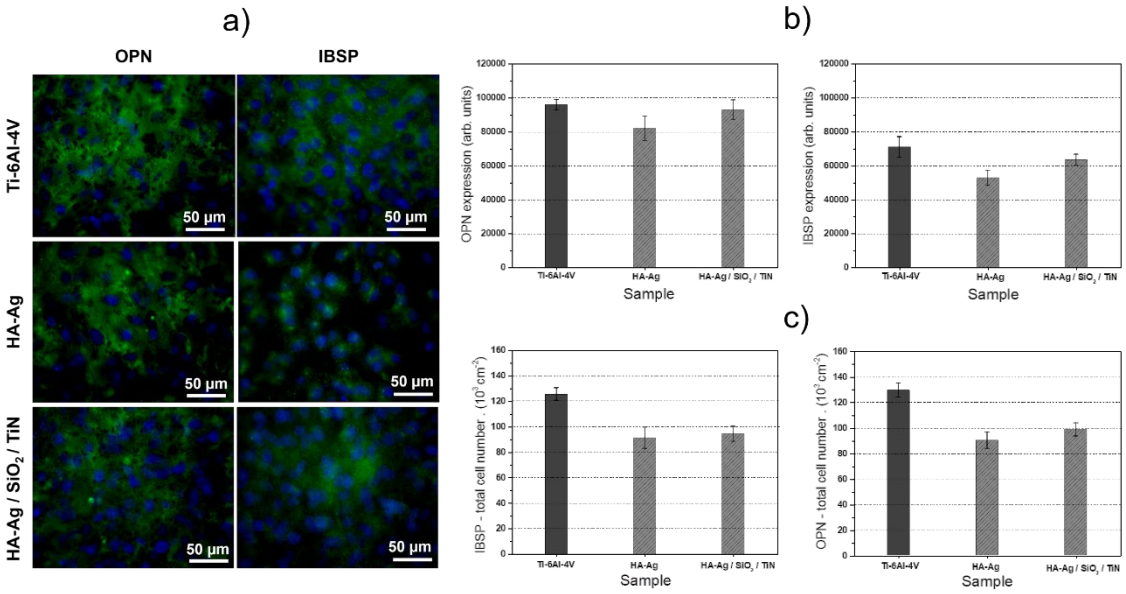

Figure 12. Differentiation of mMSCs on the different coatings and Ti-6Al-4V substrate: a) fluorescence microscopy images showing expression of OPN (green), IBSP (green) and nucleus (blue), b) quantification of OPN and IBSP staining and c) nucleus quantification. Data is represented as mean ± standard deviation.

3.7. Antibacterial properties

Figure 13 shows results of the adhesion and microbial viability assay against *S. aureus* strain carried out using Live/Dead^{TM} for the developed coatings. In Figure 13a, the bacteria with an intact cell membrane at the end of each assay time are observed in fluorescent green color, while those bacteria with a damaged membrane are shown in fluorescent red color. For the Ti-6Al-4V control, no damaged bacteria are seen during the test, which is due to the fact that this material does not have antibacterial elements, so bacteria attached there proliferate easily. For the HA-Ag coating, a large number of damaged bacteria are observed in the first evaluation at 1 h, which increases in proportion to time, and at 4 h no viable

bacteria are seen on this surface. Finally, the images of the HA-Ag/SiO_2/TiN/Ti coating showed a much slower antibacterial effect compared to the HA-Ag system, with a large number of viable bacteria observed at 1h, which slowly decreased at 2 and 4 h of evaluation. The quantification of viable and damaged bacteria in each system is presented in Figure 13b. There, it is verified that the control surface does not have antibacterial properties, while systems that incorporate Ag in their structure do. This was more evident for the HA-Ag coating obtained directly on the substrate, where a reduction close to 50% in the bacterial number was obtained at 1 h, with almost 100% of bacteria damaged at 4 h. The HA-Ag/SiO_2/TiN/Ti coating presented a milder antibacterial effect, with close to 30% damaged bacteria at 2 h of contact, which increased to 40% at 4 h. Antibacterial properties of Ag incorporated in coatings have been found in the literature for release rates higher than those registered in the present work [13,57]. M.A. Ur Rehman *et al*. [58] reported a bactericidal effect in an Ag-Si coating against the *E. coli* strain at 24 h. K. Jamuna-thevi *et al*. [59] obtained a significant antibacterial effect in Ag-TiO_2 coatings evaluated at 24 h, with a reduction close to 99% of *S. aureus* at a maximum concentration of 0.12 mg Ag/L. The antibacterial effect of Ag against the *S. aureus* strain has also been found by other authors [13,30]. Ag antibacterial properties are dependent on its size and shape. In Ag nanoparticles, the high area/volume ratio favors the release of highly reactive ions into the medium. These Ag^+ can affect the bacterial division and replication, triggering their death [30,60]. It is suggested that this mechanism could explain the results obtained in the present work.

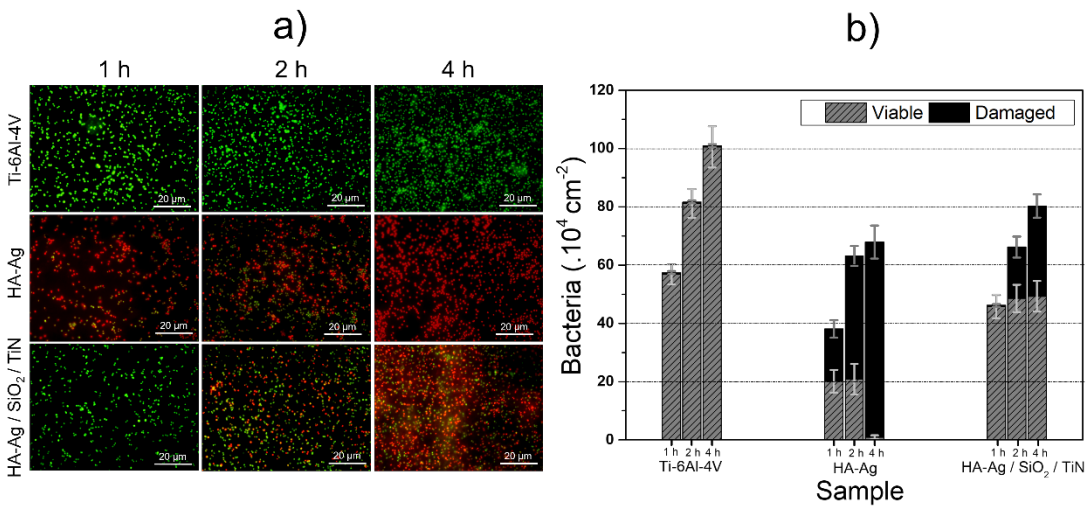

Figure 13. Microbial adhesion and viability data of *S. aureus* on the different coatings and Ti-6Al-4V substrate for 1, 2 and 4 h: a) fluorescence images showing viable bacteria (green) and damaged bacteria (red), b) quantification of adhesion and viability. Data is represented as mean ± standard deviation.

4. Conclusions

HA-Ag and HA-Ag/SiO_2/TiN/Ti multi-layer coatings with excellent compositional control (Ca/P ratio close to 1.67) were obtained. HA phase formation was confirmed by XRD, where HA characteristic peaks were observed. Furthermore, it was possible to observe through TEM the multi-layer architecture of the developed coatings. The crystallinity of the HA-Ag coating was improved by the incorporation of the SiO_2/TiN/Ti trilayer, which also enhanced the adherence to the substrate of HA-Ag by 84%. Based on the results obtained, the formation of Ag^+ as a product of the infiltration of the biological medium in the HA layers is considered a possible mechanism of Ag release. The results indicate that this process is related to the crystallinity of the HA layers and the coating architecture.

Regarding the biological response, the developed coatings presented good results in terms of viability, adhesion and differentiation of mMSCs. Furthermore, antibacterial properties against the *S. aureus* strain were obtained at concentrations < 0.25 mg Ag/L. All of the above indicates the achievement of a balance between biocompatibility and antibacterial properties, a highly desired combination on surfaces of potential application in prosthetic implants such as microplates and fixation screws.

Acknowledgements

We thank the University of Antioquia, the Centro de Investigación, Innovación y Desarrollo de materiales (CIDEMAT) group, the Departamento Administrativo de Ciencia, Tecnología e Innovación (COLCIENCIAS) for financing the Project 15-1696, the scholarship program of Enlazamundos, the Agencia de Educación Superior de Medellín (Sapiencia), JLGR acknowledges financial support from the Spanish Ministry of Economy and Competitiveness (MINECO) through the project MAT2016-76039-C4-1-R and MAT 2015-63974-C4-3-R (AEI/FEDER, UE) (including the FEDER financial support). PR acknowledges support from the Spanish Ministry of Science, Innovation and Universities (RTI2018-096794), and Fondo Europeo de Desarrollo Regional (FEDER). CIBER-BBN is an initiative funded by the VI National R&D&I Plan 2008–2011, Iniciativa Ingenio 2010, Consolider Program. CIBER Actions are financed by the Instituto de Salud Carlos III with assistance from the European Regional Development Fund. M-ERA.NET PCIN-2016-146 and RTI2018-096862-B-I00. Spanish "Junta de Extremadura" for the projects IB16117, TE-0016-18 and GR18153.

References

[1] J.J. Contreras, M. Sepúlveda, The molecular basis of infections associated to orthopedic implants., Rev. Chil. Infectología Órgano Of. La Soc. Chil. Infectología. 31 (2014) 309–22. doi:10.4067/S0716-10182014000300010.

[2] Y. Oshida, 11 - Surface Modifications, in: Y.B.T.-B. and B. of T.M. (Second E. Oshida (Ed.), Biosci. Bioeng. Titan. Mater., Elsevier, Oxford, 2013: pp. 341–456. doi:https://doi.org/10.1016/B978-0-444-62625-7.00011-X.

[3] P.I. Branemark, B.O. Hansson, R. Adell, U. Breine, J. Lindstrom, O. Hallen, A. Ohman, Osseointegrated implants in the treatment of the edentulous jaw. Experience from a 10-year period., Scand. J. Plast. Reconstr. Surg. Suppl. 16 (1977) 1–132.

[4] A. Vladescu, I. Birlik, V. Braic, M. Toparli, E. Celik, F. Ak Azem, Enhancement of the mechanical properties of hydroxyapatite by SiC addition., J. Mech. Behav. Biomed. Mater. 40 (2014) 362–368. doi:10.1016/j.jmbbm.2014.08.025.

[5] M.A. Surmeneva, R.A. Surmenev, Y.A. Nikonova, I.I. Selezneva, A.A. Ivanova, V.I. Putlyaev, O. Prymak, M. Epple, Fabrication , ultra-structure characterization and in vitro studies of RF magnetron sputter deposited nano-hydroxyapatite thin films for biomedical applications, Appl. Surf. Sci. 317 (2014) 172–180. doi:10.1016/j.apsusc.2014.08.104.

[6] M.A. Surmeneva, T.M. Mukhametkaliyev, H. Khakbaz, R.A. Surmenev, M.B. Kannan, Ultrathin film coating of hydroxyapatite (HA) on a magnesium – calcium alloy using RF magnetron sputtering for bioimplant applications, Mater. Lett. 152 (2015) 280–282.

[7] T. Yamaguchi, Y. Tanaka, A. Ide-Ektessabi, Fabrication of hydroxyapatite thin films for biomedical applications using RF magnetron sputtering, Nucl. Instruments Methods Phys. Res. Sect. B Beam Interact. with Mater. Atoms. 249 (2006) 723–725. doi:10.1016/j.nimb.2006.03.126.

[8] J. Gallo, K. Langova, V. Havranek, I. Cechova, Poor survival of ABG I hip prosthesis in younger patients., Biomed. Pap. Med. Fac. Univ. Palacky. Olomouc. Czech. Repub. 152 (2008) 163–168. doi:10.5507/bp.2008.027.

[9] S.R. Paital, N.B. Dahotre, Calcium phosphate coatings for bio-implant applications: Materials, performance factors, and methodologies, Mater. Sci. Eng. R Reports. 66 (2009) 1–70. doi:10.1016/j.mser.2009.05.001.

[10] C.S. Ciobanu, S.L. Iconaru, P. Le Coustumer, L.V. Constantin, D. Predoi, Antibacterial activity of silver-doped hydroxyapatite nanoparticles against gram-positive and gram-negative bacteria, Nanoscale Res. Lett. 7 (2012) 1–9.

[11] Q.L. Feng, J. Wu, G.Q. Chen, F.Z. Cui, T.N. Kim, J.O. Kim, A mechanistic study of the antibacterial effect of silver ions on Escherichia coli and Staphylococcus aureus, J. Biomed. Mater. Res. 52 (2000) 662–668. doi:10.1002/1097-4636(20001215)52:4<662::AID-JBM10>3.0.CO;2-3.

[12] P. Lalueza, M. Monzón, M. Arruebo, J. Santamaría, Bactericidal effects of different silver-containing materials, Mater. Res. Bull. 46 (2011) 2070–2076. doi:10.1016/j.materresbull.2011.06.041.

[13] A. Peetsch, C. Greulich, D. Braun, C. Stroetges, H. Rehage, B. Siebers, M. Köller, M. Epple, Silver-doped calcium phosphate nanoparticles: Synthesis,

characterization, and toxic effects toward mammalian and prokaryotic cells, Colloids Surfaces B Biointerfaces. 102 (2013) 724–729. doi:10.1016/j.colsurfb.2012.09.040.

[14] A.A. Yanovska, A.S. Stanislavov, L.B. Sukhodub, V.N. Kuznetsov, V.Y. Illiashenko, S.N. Danilchenko, L.F. Sukhodub, Silver-doped hydroxyapatite coatings formed on Ti-6Al-4V substrates and their characterization, Mater. Sci. Eng. C. 36 (2014) 215–220. doi:10.1016/j.msec.2013.12.011.

[15] S. Bose, H. Beyenal, A. Bandyopadhyay, L.G. Zirkle, Antimicrobial particulate silver coatings on stainless steel implants for fracture management, Mater. Sci. Eng. C. 32 (2012) 1112–1120. doi:10.1016/j.msec.2012.02.020.

[16] M. Vallet-Regí, J. Gonzalez-Calbet, Calcium Phosphates as Substitution of Bone Tissues, Prog. Solid State Chem. 32 (2004) 1–31. doi:10.1016/j.progsolidstchem.2004.07.001.

[17] R.A. Surmenev, M.A. Surmeneva, K.E. Evdokimov, V.F. Pichugin, T. Peitsch, M. Epple, The influence of the deposition parameters on the properties of an rf-magnetron-deposited nanostructured calcium phosphate coating and a possible growth mechanism, Surf. Coatings Technol. 205 (2011) 3600–3606. doi:10.1016/j.surfcoat.2010.12.039.

[18] M.A. Surmeneva, A.A. Sharonova, S. Chernousova, O. Prymak, K. Loza, M.S. Tkachev, I.A. Shulepov, M. Epple, R.A. Surmenev, Incorporation of silver nanoparticles into magnetron-sputtered calcium phosphate layers on titanium as an antibacterial coating, Colloids Surfaces B Biointerfaces. 156 (2017) 104–113. doi:10.1016/j.colsurfb.2017.05.016.

[19] K. Ozeki, T. Yuhta, H. Aoki, I. Nishimura, Y. Fukui, Crystal chemistry of hydroxyapatite deposited on titanium by sputtering technique, Biomed. Mater. Eng. 10 (2000) 221–227. http://www.scopus.com/inward/record.url?eid=2-s2.0-0033635868&partnerID=40&md5=42941a64a2b4ad2e0216f526a350a0dd.

[20] E. Mohseni, E. Zalnezhad, A.R. Bushroa, A.M. Hamouda, B.T. Goh, G.H. Yoon, Ti/TiN/HA Coating on Ti-6Al-4V for Biomedical Applications, Ceram. Int. 41 (2015) 14447–14457. doi:10.1016/j.ceramint.2015.07.081.

[21] S. Ghasemi, A. Shanaghi, P.K. Chu, Nano mechanical and wear properties of multi-layer Ti/TiN coatings deposited on Al 7075 by high-vacuum magnetron sputtering, Thin Solid Films. 638 (2017) 96–104. doi:10.1016/j.tsf.2017.07.049.

[22] D.A. Hamdi, Z.T. Jiang, K. No, M.M. Rahman, P.C. Lee, L.N.T. Truc, J. Kim, M. Altarawneh, L. Thair, T.A.J. Jumaa, B.Z. Dlugogorski, Biocompatibility study of multi-layered hydroxyapatite coatings synthesized on Ti-6Al-4V alloys by RF magnetron sputtering for prosthetic-orthopaedic implant applications, Appl. Surf. Sci. 463 (2019) 292–299. doi:10.1016/j.apsusc.2018.08.157.

[23] J. Qi, Y. Yang, M. Zhou, Z. Chen, K. Chen, Effect of transition layer on the performance of hydroxyapatite / titanium nitride coating developed on Ti-6Al-4V alloy by magnetron sputtering, Ceram. Int. 45 (2019) 4863–4869. doi:10.1016/j.ceramint.2018.11.183.

[24] J.A. Lenis, F.M. Hurtado, M.A. Gómez, F.J. Bolívar, Effect of thermal treatment on structure , phase and mechanical properties of hydroxyapatite thin fi lms grown by RF magnetron sputtering, Thin Solid Films. 669 (2019) 571–578.

doi:10.1016/j.tsf.2018.11.045.

[25] J.A. Lenis, M.A. Gómez, F.J. Bolívar, Effect of deposition temperature and target-substrate distance on the structure, phases, mechanical and tribological properties of multi-layer HA-Ag coatings obtained by RF magnetron sputtering, Surf. Coatings Technol. 378 (2019) 124936. doi:10.1016/j.surfcoat.2019.124936.

[26] A.M. Sofronia, R. Baies, E.M. Anghel, C.A. Marinescu, S. Tanasescu, Thermal and structural characterization of synthetic and natural nanocrystalline hydroxyapatite, Mater. Sci. Eng. C. 43 (2014) 153–163. doi:10.1016/j.msec.2014.07.023.

[27] H. Abrams, Grain size measurement by the intercept method, Metallography. 4 (1971) 59–78. doi:https://doi.org/10.1016/0026-0800(71)90005-X.

[28] J.A. Lenis, G. Bejarano, P. Rico, J.L.G. Ribelles, F.J. Bolívar, Development of multilayer Hydroxyapatite - Ag/TiN-Ti coatings deposited by radio frequency magnetron sputtering with potential application in the biomedical field, Surf. Coatings Technol. 377 (2019) 124856. doi:10.1016/j.surfcoat.2019.06.097.

[29] J.A. Lenis, L.J. Toro, F.J. Bolívar, Multi-layer bactericidal silver - calcium phosphate coatings obtained by RF magnetron sputtering, Surf. Coat. Technol. 367 (2019) 203–211. doi:10.1016/j.surfcoat.2019.03.038.

[30] A.M. Echavarría, P. Rico, J.L. Gómez Ribelles, M.A. Pacha-Olivenza, M.C. Fernández-Calderón, G. Bejarano-G, Development of a Ta/TaN/TaNx(Ag)y/TaN nanocomposite coating system and bio-response study for biomedical applications, Vacuum. 145 (2017) 55–67. doi:10.1016/j.vacuum.2017.08.020.

[31] A. Valverde, L. Pérez-Álvarez, L. Ruiz-Rubio, M.A. Pacha Olivenza, M.B. García

Blanco, M. Díaz-Fuentes, J.L. Vilas-Vilela, Antibacterial hyaluronic acid/chitosan multilayers onto smooth and micropatterned titanium surfaces, Carbohydr. Polym. 207 (2019) 824–833. doi:10.1016/j.carbpol.2018.12.039.

[32] A.A. Ivanova, M.A. Surmeneva, I.Y. Grubova, A.A. Sharonova, V.F. Pichugin, M. V. Chaikina, V. Buck, O. Prymak, M. Epple, R.A. Surmenev, Influence of the substrate bias on the stoichiometry and structure of RF-magnetron sputter-deposited silver-containing calcium phosphate coatings, Materwiss. Werksttech. 44 (2013) 218–225. doi:10.1002/mawe.201300101.

[33] M.A. Surmeneva, M. V. Chaikina, V.I. Zaikovskiy, V.F. Pichugin, V. Buck, O. Prymak, M. Epple, R. a. Surmenev, The structure of an rf-magnetron sputter-deposited silicate-containinghydroxyapatite-based coating investigated by high-resolution techniques, Surf. Coatings Technol. 218 (2013) 39–46. doi:10.1016/j.surfcoat.2012.12.023.

[34] V. Nelea, C. Morosanu, M. Iliescu, I.N. Mihailescu, Microstructure and mechanical properties of hydroxyapatite thin films grown by RF magnetron sputtering, Surf. Coatings Technol. 173 (2003) 315–322. doi:10.1016/S0257-8972(03)00729-1.

[35] M. Polok, M. Adamiak, Structure and properties of wear resistance PVD coatings deposited onto X37CrMoV5-1 type hot work steel, Mater. Process. Technol. 165 (2005) 843–849. doi:10.1016/j.jmatprotec.2005.02.164.

[36] S.J. Ding, C.P. Ju, J.H.C. Lin, Characterization of hydroxyapatite and titanium coatings sputtered on Ti-6Al-4V substrate, J. Biomed. Mater. Res. 44 (1999) 266–279. doi:10.1002/(SICI)1097-4636(19990305)44:3<266::AID-JBM5>3.0.CO;2-4.

[37] A.A. Ivanova, M.A. Surmeneva, A.I. Tyurin, T.S. Pirozhkova, I.A. Shuvarin, O. Prymak, M. Epple, M. V. Chaikina, R.A. Surmenev, Fabrication and physico-mechanical properties of thin magnetron sputter deposited silver-containing hydroxyapatite films, Appl. Surf. Sci. 360 (2016) 929–935. doi:10.1016/j.apsusc.2015.11.087.

[38] E. Contreras Romero, J. Cortínez Osorio, R. Talamantes Soto, A. Hurtado Macías, M. Gómez Botero, Microstructure, mechanical and tribological performance of nanostructured TiAlTaN-(TiAlN/TaN)n coatings: Understanding the effect of quaternary/multilayer volume fraction, Surf. Coatings Technol. 377 (2019) 124875. doi:10.1016/j.surfcoat.2019.07.086.

[39] D. Deligianni, N. Katsala, S. Ladas, D. Sotiropoulou, J. Amedee, Y. Missirlis, Effect of surface roughness of the titanium alloy Ti-6Al-4V on human bone marrow cell response and on protein adsorption., Biomaterials. 22 (2001) 1241–51. doi:10.1016/S0142-9612(00)00274-X.

[40] A. Zareidoost, M. Yousefpour, B. Ghaseme, A. Amanzadeh, The relationship of surface roughness and cell response of chemical surface modification of titanium, J. Mater. Sci. Mater. Med. 23 (2012) 1479–1488. doi:10.1007/s10856-012-4611-9.

[41] M.A. Surmeneva, A.I. Tyurin, T.M. Mukhametkaliyev, T.S. Pirozhkova, I.A. Shuvarin, M.S. Syrtanov, R.A. Surmenev, Enhancement of the mechanical properties of AZ31 magnesium alloy via nanostructured hydroxyapatite thin films fabricated via radio-frequency magnetron sputtering, J. Mech. Behav. Biomed. Mater. 46 (2015) 127–136. doi:10.1016/j.jmbbm.2015.02.025.

[42] A. Quirama, A.M. Echavarría, J.M. Meza, J. Osorio, G. Bejarano G, Improvement of the mechanical behavior of the calcium phosphate coatings deposited onto Ti6Al4V alloy using an intermediate TiN/TiO2 bilayer, Vacuum. 146 (2017) 22–30. doi:https://doi.org/10.1016/j.vacuum.2017.09.024.

[43] E.S. Thian, J. Huang, Z.H. Barber, S.M. Best, W. Bonfield, Surface modification of magnetron-sputtered hydroxyapatite thin films via silicon substitution for orthopaedic and dental applications, Surf. Coatings Technol. 205 (2011) 3472–3477. doi:10.1016/j.surfcoat.2010.12.012.

[44] M. Surmeneva, C. Kleinhans, G. Vacun, P. Kluger, V. Schönhaar, M. Müller, S.B. Hein, A. Wittmar, M. Ulbricht, O. Prymak, C. Oehr, O. Surmenev, Nano-hydroxyapatite coated metal ceramic composite of iron tricalcium Phosphate : improving the surface wettability, adhesion and proliferation of mesenchymal stem cells in vitro, Colloids Surfaces / B Biointerfaces. 135 (2015) 386–393. doi:10.1016/j.colsurfb.2015.07.057.

[45] W. Chen, Y. Liu, H.S. Courtney, M. Bettenga, C.M. Agrawal, J.D. Bumgardner, J.L. Ong, In vitro anti-bacterial and biological properties of magnetron co-sputtered silver-containing hydroxyapatite coating., Biomaterials. 27 (2006) 5512–7. doi:10.1016/j.biomaterials.2006.07.003.

[46] ASTM C1624-05, Standard Test Method for Adhesion Strength and Mechanical Failure Modes of, Astm. 05 (2015) 1–29. doi:10.1520/C1624-05R15.Scope.

[47] W. Boonrawd, M. Hamdi, A. Shukor, T.C. Yong, Radio Frequency Magnetron Sputtering HA / Ti Coatings Deposited Using Double-Layered Target: Phase

Composition and Film Adherence of Heat-Treated Coatings, in: 11th Asia Pacific Ind. Eng. Manag. Syst. Conf., 2010: pp. 7–10.

[48] Y. Chen, X. Zheng, Y. Xie, H. Ji, C. Ding, H. Li, K. Dai, Silver release from silver-containing hydroxyapatite coatings, Surf. Coatings Technol. 205 (2010) 1892–1896. doi:10.1016/j.surfcoat.2010.08.073.

[49] L. Actis, L. Gaviria, T. Guda, J.L. Ong, Antimicrobial surfaces for craniofacial implants: state of the art., J. Korean Assoc. Oral Maxillofac. Surg. 39 (2013) 43–54. doi:10.5125/jkaoms.2013.39.2.43.

[50] J. Parvizi, T. Gehrke, Periprosthetic Joint Infection: current concept, Indian J. Orthop. 47 (2013) 10–17.

[51] M. Salmerón-Sánchez, P. Rico, D. Moratal, T.T. Lee, J.E. Schwarzbauer, A.J. García, Role of material-driven fibronectin fibrillogenesis in cell differentiation, Biomaterials. 32 (2011) 2099–2105. doi:10.1016/j.biomaterials.2010.11.057.

[52] S.A. Redey, M. Nardin, D. Bernache-Assolant, C. Rey, P. Delannoy, L. Sedel, P.J. Marie, Behavior of human osteoblastic cells on stoichiometric hydroxyapatite and type A carbonate apatite: role of surface energy., J. Biomed. Mater. Res. 50 (2000) 353–364.

[53] S. Spriano, M. Bosetti, M. Bronzoni, E. Verne, G. Maina, V. Bergo, M. Cannas, Surface properties and cell response of low metal ion release Ti-6Al-7Nb alloy after multi-step chemical and thermal treatments., Biomaterials. 26 (2005) 1219–1229. doi:10.1016/j.biomaterials.2004.04.026.

[54] E.A. Vogler, Water and the acute biological response to surfaces, J. Biomater. Sci.

Polym. Ed. 10 (1999) 1015–1045. doi:10.1163/156856299X00667.

[55] J.Y. Lim, X. Liu, E.A. Vogler, H.J. Donahue, Systematic variation in osteoblast adhesion and phenotype with substratum surface characteristics, J. Biomed. Mater. Res. 68A (2004) 504–512. doi:10.1002/jbm.a.20087.

[56] C. Sengstock, J. Diendorf, M. Epple, T. a Schildhauer, M. Köller, Effect of silver nanoparticles on human mesenchymal stem cell differentiation., Beilstein J. Nanotechnol. 5 (2014) 2058–69. doi:10.3762/bjnano.5.214.

[57] J.M. Sahuquillo Arce, A. Iranzo Tatay, M. Llácer Luna, Y. Sanchis Boix, J. Guitán Deltell, E. González Barberá, J. Beltrán Heras, M. Gobernado Serrano, Estudio in vitro de las propiedades antimicrobianas de una espuma de poliuretano que libera iones de plata, Cir. Esp. 89 (2011) 532–538. doi:10.1016/j.ciresp.2011.02.015.

[58] M.A. Ur Rehman, S. Ferraris, W.H. Goldmann, S. Perero, F.E. Bastan, Q. Nawaz, G.G. Di Confiengo, M. Ferraris, A.R. Boccaccini, Antibacterial and Bioactive Coatings Based on Radio Frequency Co-Sputtering of Silver Nanocluster-Silica Coatings on PEEK/Bioactive Glass Layers Obtained by Electrophoretic Deposition, ACS Appl. Mater. Interfaces. 9 (2017) 32489–32497. doi:10.1021/acsami.7b08646.

[59] K. Jamuna-thevi, S.A. Bakar, S. Ibrahim, N. Shahab, M.R.M. Toff, Quantification of silver ion release , in vitro cytotoxicity and antibacterial properties of nanostuctured Ag doped TiO 2 coatings on stainless steel deposited by RF magnetron sputtering, Vaccum. 86 (2011) 235–241. doi:10.1016/j.vacuum.2011.06.011.

[60] S. Chernousova, M. Epple, Silver as antibacterial agent: Ion, nanoparticle, and metal, Angew. Chemie - Int. Ed. 52 (2013) 1636–1653. doi:10.1002/anie.201205923.